

Enhancement of inline mixing with lateral synthetic jet pairs at low Reynolds numbers: The effect of fluid viscosity

Qingfeng Xia^{1,2} and Shan Zhong^{1*}

¹School of Mechanical, Aerospace and Civil Engineering,
University of Manchester, Manchester, M13 9PL UK

²Department of Engineering Science, University of Oxford, Oxford, OX1 3PJ, UK

*Email: shan.zhong@manchester.ac.uk

Abstract

In this paper, mixing between two liquid streams of the same flow rate in a planar mixing channel enhanced by means of three lateral synthetic jet pairs is examined using PLIF and PIV at net flow Reynolds numbers of $Re_n=2, 10$ and 83 . The changes in the flow Reynolds numbers are produced with the use of fluids with different dynamic viscosities. The synthetic jet pairs are operated 180° out-of-phase and at a range of actuation frequencies (characterized by the dimensionless Strouhal number Str) and displacements (characterized by the dimensionless stroke length L). It is found that at a sufficiently high frequency or dimensionless stroke length, a homogenous mixing can be achieved. Our experimental evidence shows that the synthetic jet pairs enhance mixing via two key mechanisms, i.e. vortex interaction and entrainment; tearing and stretching of liquid interface. A functional relationship among Re_n , Str and L to ensure a nearly homogenous mixing is also obtained by best fitting the experimental data. It can be used for selecting the synthetic jet operating conditions to ensure a good mixing for a scaled version of this fluid mixer. This correlation indicates that the effectiveness of mixing has a weak dependence on Re_n , implying that the fluid mixers of such a design can be effective over a wide range of net flow Reynolds numbers and for fluids of different viscosities.

Keywords: Synthetic jets, jet mixing, liquid mixing, PLIF, PIV, low Reynolds numbers

1. Introduction

Jet mixing is referred to a class of mixing techniques, which make use of a suitable arrangement of jets to achieve rapid inline mixing. It offers an advantage of structural simplicity in the design of fluid mixers. Jet mixing may involve a use of passive mixing techniques, such as collision of jets [1] and eddy formation, and active mixing techniques, such as periodic injection switching [2] and periodic lateral perturbation [2]. In jet mixing, sequential segmentation generated by out-of-phase periodic injection can enhance mixing effectively [3]. Sequential segmentation is a process where solvent and solute streams are broken up into segments in the axial direction, which subsequently increases the interfacial areas and hence promotes mixing.

Despite the volume of research work on jet mixing [1, 4, 5], however, the degree of mixing is often found undesirable at Reynolds numbers below a few hundreds. Hence, there is a need for developing new mixing techniques, which are effective at lower Reynolds numbers. Such a progress will be beneficial to the development of effective devices for mixing in many applications, such as inline flow mixers for very viscous fluids and bi-sensors, in which the level of mixing is suppressed by their inherent low Reynolds numbers.

A synthetic jet can be created by an oscillating diaphragm attached to a cavity with an orifice opening. It has a unique feature of injecting vorticity and momentum into a flow field without the need of an external fluid source [6-8]. Despite the large volume of research carried out on synthetic jets, which is largely focused on flow separation control and heat transfer enhancement over solid surfaces [9-11], their use in enhancing fluid mixing has been much less well explored. Synthetic jets which are issued transversely into an oncoming flow in a

channel are capable of generating intensive local disturbances and hence enhancing mixing. Furthermore, the strength of synthetic jets can be varied independently from that of the main flow to enable mixing in low Reynolds number flows where turbulence is absent.

Recently, the authors of this paper have successfully demonstrated the use of a single lateral synthetic jet pair in enhancing mixing between two fluid streams at a net flow Reynolds number of 83 [12, 13]. The synthetic jet pair is located on the opposite side-walls of a rectangular mixing channel. At relatively high synthetic jet actuation frequencies or amplitudes, homogeneous mixing is achieved downstream of the jet orifices. As the Reynolds number reduces, it becomes increasingly more difficult to fully mix fluids using a single jet pair due to lack of vortical structures. With the use of three lateral synthetic jet pairs, however, the authors showed that a homogenous mixing can also be obtained at a net flow Reynolds number as low as 2 [14]. To the best knowledge of the authors, the aforementioned work represents the first successful application of synthetic jets in enhancing fluid mixing at low Reynolds numbers.

In this paper, the mixing process between two liquid streams enhanced by using three lateral synthetic jet pairs are examined collectively over a range of net flow Reynolds numbers ($Re_n = 2 \sim 83$). The purpose of this work is to investigate the changes in the key mixing mechanisms and deduce a functional relationship between Re_n and the other dimensionless parameters characterising the synthetic jet operating parameters, which ensures a homogenous mixing. Although when the geometry of the fluid mixer is fixed, the net Reynolds numbers can be altered by changing either the net flow velocity in the mixing channel or the fluid viscosity, in this study changes in the net Reynolds numbers are introduced with the use of liquids with different dynamic viscosities. Such a choice is based on the consideration that a) fluid with a

higher viscosity is more challenging to mix due to the inherent low jet Reynolds number even though the jet velocity of the synthetic jets can be adjusted independently from that of the net flow; b) The finding from this work will be useful for developing a class of industrial fluid mixers required for mixing fluids with a range of viscosities.

2. Experimental setup and methods

2.1 The fluid mixer and synthetic jet actuators

A schematic of the fluid mixer used in the present study is shown in **Fig. 1**. Two fluid streams are introduced into the mixing channel via a confluence inlet. The rectangular mixing channel, which is made of Perspex, has a width of $h = 0.008$ m, a depth of $w = 0.040$ m and a length of 1 metre. Lateral perturbations are introduced transversely into the mixing channel via synthetic jet pairs located on the two opposite side walls of the mixing channel. The jet orifice has a width of $d = 0.004$ m and spans the entire depth of the channel. The ratio between the orifice width and the channel width, d/h , is 0.5. A relatively high value of d/h , such as the one used here, ensures the formation of vortices with a size comparable to the mixing channel width hence the mixing effectiveness of the synthetic jets. The spacing between the centres of adjacent orifices is chosen to be 0.016 m, which is equivalent to $2h$. The choice of such spacing is to ensure that the orifices along the same wall are close to each other, but at the same time the vortices produced from the adjacent orifices do not interface with each other resulting in weakened structures.

The three synthetic jets located on the same side-wall of the mixing channel share the same cavity, which has an inner dimension of 0.126 m x 0.126 m x 0.010 m. A circular oscillating piston, which is made of a thin rubber sheet sandwiched between two thin metal disks of 0.120 m in diameter, is clamped circumferentially to the back of each cavity. The pistons of

both cavities are connected to a single magnetic shaker via a rigid metal frame (see **Fig. 1(a)**) and they oscillate in a sinusoidal manner at a predetermined displacement and frequency. The metal frame is supported and aligned with the aid of two linear bearings to ensure that the displacement of the shaker is transmitted to the two pistons as evenly as possible. With the above mechanical arrangement, the left synthetic jets and the right synthetic jets will operate 180° out-of-phase and hence the instantaneous flow rate downstream of the jet pairs in the mixing channel will not change with time.

2.2 Experimental methods

In this study, the **PLIF** technique is employed to provide both a qualitative and quantitative assessment of the extent of mixing in the mixing channel. PIV measurements of the flow fields are also undertaken so as to provide complementary information about the presence of vortices produced by the synthetic jets and their role in promoting mixing as well as the downstream velocity profile across the width mixing channel required for quantification of the mixing degree.

In the PLIF measurements, the light sheet produced by a New Wave™ Nd-YAG 532nm pulsed laser is used to illustrate the flow field on the central plane of the mixing channel (see **Fig.1**). The laser light is directed into the channel by a small mirror set at a 45° angle to the flow direction. The mirror is inserted into the channel at a distance of $26h$ (0.208 m) downstream of the centre of the synthetic jet cavity. Although it spans across the 0.008 m width of the mixing channel, its depth of 0.004 m counts for only 10% of the channel depth. Therefore the mirror is expected to have a negligible effect on the upstream flow field. This is also confirmed in our CFD simulation of the flow field which is not shown here. A **CCD** camera fitted with a high-pass optical filter, which lets through the light emitted by the fluorescence

dye while filters out the laser light, is used to capture the **PLIF** images. The TSI POWERVIEW™ Plus 4MP model 630059 camera has a maximum resolution of 2048×2048 pixels and a pixel size of $7.4 \mu\text{m} \times 7.4 \mu\text{m}$. Hollow glass spheres with a mean diameter of $10 \mu\text{m}$ and an equivalent density of 1.1 g/cm^3 , are seeded into the liquid. The camera is focused onto the laser sheet plane with a viewing area of $8\text{mm} \times 40\text{mm}$ utilizing a high standard Micro-Nikkon AF 60 mm f2.8D lens. A synchronizer (LASERPULSE™ model 610034) and Insight 3G™ software from TSI Inc are used to control the firing of the laser and trigger the camera. The experimental instrumentation used for PIV is identical to that used in PLIF experiment except that the fluorescence optical filter is omitted.

In the present experiment, eighty phase-locked PLIF and PIV images are acquired at each of the eight equally spaced phases in the synthetic jet actuation cycle, from which phase-averaged velocity fields are obtained. The uncertainties in the dye concentration and velocity measurements are estimated to be less than 2% and 3%, respectively. Detailed description of the experimental setup for PLIF and PIV can be found in Xia [15].

2.3 Quantitative evaluation of the degree of mixing

The quantitative evaluation of the extent of mixing is based on the velocity-weighted coefficient of variation in the Rhodamine B concentration profile [16], which is defined in the following equation,

$$\text{Mixing degree} = 1 - CoV = 1 - \sqrt{\frac{\int_{-h/2}^{h/2} \left(\frac{c}{\bar{c}} - 1\right)^2 \frac{u}{\bar{u}} dx}{h}} \quad (1)$$

where CoV is coefficient of variation, \bar{u} is the mean streamwise velocity at a chosen cross-section and a given phase during an actuation cycle, u is the local phase-averaged streamwise

velocity, c is the local Rhodamine B concentration and \bar{c} is the Rhodamine B concentration at the fully mixed condition. For simplicity, the normalised velocity profile across the section u/\bar{u} is assumed to be parabolic.

In the present experiment the extent of mixing is evaluated at $y=12.5h$, which is 0.1 m downstream from the centre of the synthetic jet cavities (The coordinate system is defined in Fig. 1). A single representative value of mixing degree at this location is obtained by firstly averaging the eighty **PLIF** images acquired at a frequency of 3.7 Hz and then averaging across the entire width of the channel.

2.4 Test conditions

The dimensionless analysis carried out in [14] reveals that, for a given multiple synthetic jet pair configuration, the level of mixing in the mixing channel is determined by three independent dimensionless parameters. They are the net flow Reynolds number, $Re_n = \rho h \bar{U}_n / \mu$, the dimensionless stroke length, $L = \bar{U}_j / fd$, the Strouhal number, $Str = fd / \bar{U}_n$. Here, \bar{U}_n is the mean flow velocity in the mixing channel deduced from the reading on a positive displacement volumetric flow rate meter, and \bar{U}_j is the synthetic jet mean blowing velocity over its actuation cycle, which can be estimated by the measured piston oscillating amplitude, the adjustable actuation frequency and the actuator geometry [14]. Both U_n and U_j are spatially averaged across the corresponding cross section.

Two other dimensionless parameters are also widely used in characterising synthetic jets. They are the velocity ratio

$$R_v = \frac{\bar{U}_j}{\bar{U}_n} = L \cdot Str \quad (2)$$

which represents the relative strength of the synthetic jet to the mean flow, and the jet Reynolds number which is given by

$$\text{Re}_j = \frac{\rho \bar{U}_j d}{\mu} = R_v \text{Re}_n \frac{d}{h} \quad (3)$$

As illustrated in **Eqs. 2 and 3**, however, neither R_v nor Re_j is independent of Re_n , L , and Str .

In this experiment, the flow rate in the mixing channel is kept the same and the net flow Reynolds number is altered by using pure water and cane sugar solutions with two different mass fractions. A cane sugar solution is Newtonian fluid for a sugar concentration up to 78% [17], and its viscosity is predictable given the sugar mass fraction and temperature [18]. The properties of the fluids used in this experiment are given in Table 1.

Table 1 Physical property of different liquids used in the experiment at 20°C

	Pure water	Sugar solution 1	Sugar solution 2
Sugar mass fraction	0	0.447	0.582
Density (kg/m ³)	998	1248	1260
Dynamic viscosity (Pa·s)	1.0×10 ⁻³	1.0×10 ⁻²	4.8×10 ⁻²

During the experiment, the flow rate ratio of the two fluid streams to be mixed in the mixing channel is kept as 1 and the mean velocity in the channel is fixed at 0.01 m/s. The use of pure water and sugar solutions with two different sugar mass concentrations gives a net flow Reynolds number of 2, 10 and 83 respectively. In order to evaluate the influence of the lateral synthetic jets operating parameters on mixing, the peak-to-peak displacement and frequency of the synthetic jet actuators are varied independently from 0.1 to 0.6 mm and from 1 to 10 Hz respectively. The corresponding dimensionless stroke length varies from 1 to 8, and the Strouhal number from 0.4 to 3.2.

3. Experimental results

3.1 $Re_n=83$

Figure 2 shows a time sequence of the velocity vector fields superimposed with vorticity contours obtained during a synthetic jet actuation cycle at $f=1\text{Hz}$ and $L=4$. Since the velocity patterns at the second half of the synthetic jet actuation cycle are symmetrical relative to the central plane of the mixing channel, only the first half of the actuation cycle is presented here. The three left jets are in the ejection cycle, whereas the three right jets are in the ingestion cycle. At $t=0$, the pistons of both the left and right cavity are at their left most position and they are about to move to the right to initiate the corresponding ejection and ingestion cycle of the respective actuator respectively (Fig. 2(a)). At this moment, the vortex pairs produced by the right actuator in its previous actuation cycle appear to dominate the mixing channel. At $t=1/8T$, as the piston of the left cavity moves towards its orifices, some fluid inside is pushed out of the left cavity as indicated by the velocity vectors at the exits of the left orifices (Fig. 2(b)). At the same time, the piston of the right cavity is moving away from its orifices, inhaling the ambient fluid into the right cavity. As such, a jet flow directing from the left orifices towards the right orifices is formed. At $t=1/4T$, as both the left and right piston just reach their neutral position with the maximum injection and ingestion velocity being acquired at the left and the right orifices respectively. The vortex pairs produced by the ejection cycle of the left actuator continue to grow in size (Fig. 2(c)). By $t=1/2T$, these vortex pairs have gained the maximum strength and become the dominant features in the mixing channel (Fig. 2I). At this instant, both the left and right pistons just reach their right most positions, and the ejection and ingestion cycle of the two actuators is about to be reversed which will subsequently result in formation of a jet flow towards the left wall (the second half cycle is not shown here).

In Fig. 3, a time sequence of the PLIF images for the same case presented in Fig. 2 is shown. At $t=0$, the left fluid stream with high dye concentration (in red) and the right fluid stream with no dye concentration (in dark blue) are seen to enter the mixing channel in parallel just upstream of the first jet pair (Fig. 3(a)). At $t=1/8T$ (Fig. 3(b)), the ejection cycle of the left jets has already begun and a small vortical structure is seen to emerge from the first left orifice (labelled as **A**). Due to ingestion from the right orifice, a portion of the left fluid stream in red is being inhaled along with the fluid in dark blue in the right fluid stream by the first right orifice, causing the left fluid stream to arch across the entire width of the mixing channel. As the above process continues, structure **A** continues to grow. In particular, the downstream branch of structure **A** is strengthened by the local shear and is seen to entrain the ambient fluid into its core (Fig. 3(d)). Beginning at $t=1/2T$, the ingestion cycle of the left jets starts (Fig. 3(e)). A portion of the left fluid stream in red is seen being drawn into the left jet orifice at $t=5/8T$ (Fig. 3(f)). At $t=3/4T$, as the ingestion cycle of the left jets progresses a portion of the right fluid stream in blue is also drawn into the left jet orifice, chopping structure **A** off its stem (Fig. 3(g)). At the same time, a vortical structure (labelled as **B**), which has already emerged from the right jet orifice, grows in size. The downstream branch of structure **A** and **B** combine with each other to form a vortex pair (see Fig. 3(h)), which is carried downstream by the net flow in the mixing channel. It also can be seen that structure **B** ejected from the first right orifice has a lower dye concentration than the ambient fluid. This is because that fluids with both high and low dye concentrations have been inhaled into the right cavity earlier and some levels of mixing have taken place inside the right cavity.

The development of structure **A** and **B** further downstream can be examined by following the same structures produced during the previous actuation cycles. Both structures are seen to entrain the ambient fluid into their cores as they propagate downstream in the mixing channel.

Structure B can be traced from Figs. 3(a-g) till it arrives at the second right orifice and it is then significantly weakened by the structure ejected from the second right orifice. Structure A can be traced from Figs. 3(a-g) too. It is firstly squeezed by the newly formed structure ejected by the second left orifice. It is then partly inhaled into the second left orifice. Clearly, the impact of actuation of the second jet pair on the structures produced by the first jet pair leads to further improvement in mixing as indicated by the green colour in the local dye concentration contours. Similarly, the vortical structure (Structure C in Fig. 3(c)) produced by the ejection cycle of the second left jet orifice can be traced until it is inhaled by the third left orifice in Fig. 3(f). Finally, it can be seen in Fig. 3(b) that the vortex pair D produced by the third left orifice emerges at $t=1/8T$ and it hits the opposite wall at $t=1/2T$ as it grows in size (Fig. 3(e)). The upstream branch of the vortex pair appears to consist of fluid with high dye concentration due to some residuals of unmixed fluid in the cavity. Its upstream branch in red becomes disintegrated upon an interaction with the structure produced by the ejection cycle of the third right orifice, Fig. 3(h). Further downstream, the mixing channel appears to be filled with weak downstream branches of the vortex pairs produced by the third jet pair.

In Fig. 4, velocity vector fields superimposed with vorticity contours obtained at $f=1\text{Hz}$ for a range of dimensionless stroke lengths from $L=2$ to 8 are presented for the phase $t=1/2T$. It can be seen that the strength of the vortex pairs increase progressively as L increases. The dye concentration patterns at an actuation frequency of 1Hz and at a range of dimensionless stroke lengths from $L=0$ to 6 obtained at the same phase are shown in Fig. 5. At $L=0$, there is no mixing between the two fluid streams except at their interface where mixing at the molecular level takes place (Fig. 5(a)). At $L=1$, due to a low strength of the synthetic jets, the fluid is only disturbed to give rise to a wavy interface (Fig. 5(b)). At $L=2$, the jet structures just manage to reach the opposite wall resulting in a limited level of mixing (Fig. 5(c)). As the

dimensionless stroke length increases, the level of mixing improves progressively. At $L=6$, an almost homogenous mixing is achieved right after the first jet pairs (Fig. 5(g)).

3.2 $Re_n=10$

In Fig.6, a time sequence of the velocity vector fields superimposed with vorticity contours obtained during a synthetic jet actuation cycle at the intermediate Reynolds number of $Re_n=10$ is shown. It is found that although the velocity vector fields reveal regions of low vorticity produced by the synthetic jet pairs and creation of local flow towards orifices at certain phases of an actuation cycle (see Fig. 6), well defined vortical structures observed at $Re_n=83$ are absent. Despite the same actuation frequency and amplitude as in Fig. 3 being used, since the viscosity of the fluid is higher the jet Reynolds number is lower hence suppressing the rollup of vortices.

The above observation is consistent with the dye concentration contours shown in Fig. 7. Structure A in red originated from a portion of the high dye concentration fluid (Fig. 7(b)) is stretched across the mixing channel by the ingestion cycle of the right cavity (Fig. 7(b)-(e)) and it is then chopped off stem by the subsequent ingestion cycle of the left cavity (Fig. 7(f)). Structure A can be traced for one more actuation cycle as it propagates downstream during which it is subjected to further stretching due to the local shear in the mixing channel. It is eventually destroyed by the second right orifice during its injection cycle (Fig. 7(c)). Structure B in blue (Fig. 7(a)-(c)) is produced in a similar way but by the ingestion cycle of the left cavity. It also disappears when it is inhaled into the second right orifice during its ingestion cycle (Fig. 7(f)). The level of mixing is already quite good when the flow reaches the second jet pair. Structure D (Fig. 7g)) is produced by the second right jet whereas structure C (Fig. 7(b)) by the second left jet. They are combined to form structure E (Fig.

7(d)) which eventually disappears into the left orifice of the third jet pair. The structure produced by the third left jet orifice is seen as structure F (Fig. 7(b)) and it remains faintly visible further downstream.

Overall, it can be seen that the out-of-phase actuation of the first orifice pair essentially serves to stretch and tear the incoming fluid into segments of high and low dye concentration and release them into the main flow in an alternative manner. These fluid segments are then subjected to further stretching by shear as they propagate downstream in the channel and undergo further mixing as they go through the subsequent jet orifices. The structures ejected by the second and third orifice pairs appear to have progressively lower dye concentration than that of the structures upstream, indicating the effectiveness of the mixing process which has taken place in between.

The instantaneous dye concentration contours obtained at $f=1\text{Hz}$ and at a range of dimensionless stroke lengths from $L=1$ to 6 obtained at the phase $t=1/2 T$ again illustrate the progressive improvement of mixing as L increases, see Fig. 8. A nearly homogeneous mixing is achieved at $L=6$ before the fluid reaches the second jet pairs.

3.3 $Re_n=2$

The time sequence of velocity vector field for $f=1\text{Hz}$ and $L=6$ at $Re_n=2$ is shown in Fig. 9. The absence of well-defined vortex rollup is also evident. At $Re_n=2$, the dye concentration patterns obtained at different L and $f=1\text{Hz}$ appear similar to those seen at $Re_n=10$, except that a slightly worse mixing is evident such that the fluid ejected from the second and third orifice

pairs is less well mixed (compare Fig. 10 with Fig. 8). Nevertheless, a reasonably good mixing is still achieved at the location of the third jet pair with $L=7$ (Fig. 10(g)).

Interestingly, the disturbance produced by the synthetic jet pairs appears to be greater at $L \leq 2$ at the two lower Reynolds numbers, i.e. $Re_n=2$ and 10. For the synthetic jet pairs with an orifice to channel width ratio of 0.5 used in the present study, the disturbances produced by the synthetic jets with $L < 2$ are unable to reach the opposite wall disregard of the magnitude of Re_n , resulting in a limited level of mixing in the channel. Based on the study by Zhou et al. [6], the extent of vortex roll-up in a synthetic jet is determined by the shape of the orifice exit velocity profile hence by the Stokes number which is defined as $St = \sqrt{\frac{2\pi f d^2}{\nu}}$. A top-hat velocity profile accompanied by a thin Stokes layer due to the use of a higher Stokes number encourages vortex roll-up, whereas a parabolic profile with a thick Stokes layer extending to the centre of the orifice inhibits the roll-up. At $Re_n=83$, vortex rollup is visible at the orifice exit whereas it is absent at $Re_n=2$ and 10. Hence the exit velocity profile at $Re_n=2$ and 10 is likely to have a parabolic shape, whereas at $Re_n=83$ the velocity profile may have a top-hat shape. As such, at the same L the maximum velocity at the centre of the orifice at $Re_n=2$ and 10 is higher, leading to a slightly deeper penetration across the width the channel.

3.4 Functional relationship for ensuring good mixing

In order to compare the extent of mixing at different synthetic jet operating conditions quantitatively, the time-averaged degree of mixing at $y=12.5h$ is deduced from the **PLIF** measurement on the mid-plane across the depth of the mixing channel. It should be noted that the degree of mixing is evaluated at a distance of $7.5h$ downstream of the end of the

measurement window of the PLIF images presented earlier. Hence the level of mixing is expected to be slightly better as a result of further stretching of fluid elements due to shear.

Figure 11 presents the variations of degree of mixing with the dimensionless stroke length at $f=1\text{Hz}$ and $\text{Re}_n=2, 10$ and 83 . It appears that at $L \leq 2$ the level of mixing is low at these Reynolds numbers. However, at intermediate values of L the level of mixing improves as the net Reynolds number increases. Nevertheless, it eventually becomes similarly good again when L exceeds 6.

In order to obtain a correlation for the synthetic jet operating conditions at which a good mixing is guaranteed, for a given Re_n a best fit curve is found for the relationship between the degree of mixing and the dimensionless stroke length at each frequency. The value of L at a degree of mixing equal to 0.9 is then extracted from the best fit curve for each frequency. **Table 2** lists the dimensionless parameters at which a mixing degree of 0.9 is achieved for a range of synthetic jet operating conditions at $\text{Re}_n=2, 10$ and 83 respectively.

From Table 2, one can see that the minimum value of L to ensure a good mixing is close to 2. This is a manifestation of the need for the synthetic jet to penetrate the width of the mixing channel during an actuation cycle. It is also obvious that at a given Re_n a lower Str can be used in conjunction with a higher L or vice versa to produces a good mixing. Over the range of Re_n examined, the range of L and Str , which allows a good mixing to be achieved is roughly the same, indicating a weak dependence on Re_n . The fact that all the value of R_v listed in Table 2 is greater than unity suggests that the intensity of perturbation produced by the synthetic jets needs to have a sufficient strength which matches that of the flow in the

channel. Nevertheless, there is a slight reduction in R_v to produce the same level of mixing as Re_n increases.

**Table 2 Parameters table for achieving degree of mixing of 0.9
with three lateral synthetic jet pairs**

Re_n	L	Str	R_v	Re_j
83	3.4	0.4	1.4	57.1
83	2.6	0.8	2.1	86.7
83	2.4	1.2	2.9	118.5
83	2.3	1.6	3.6	151.4
83	2.2	2.4	5.2	217.1
83	1.8	3.2	5.7	237.7
10	4.7	0.4	1.9	9.5
10	3.6	0.8	2.9	14.6
10	2.0	3.2	6.5	32.3
2	5.5	0.4	2.2	2.2
2	3.9	0.8	3.1	3.1
2	2.9	1.2	3.5	3.5
2	2.6	1.6	4.2	4.2
2	2.3	2.4	5.5	5.5
2	1.9	3.2	6.1	6.1

A correlation for Re_n , L and Str at which a good mixing is achieved can then be proposed as below,

$$Re_n^i L^j Str = A \quad (4)$$

where A is a constant, i and j are exponents of Re_n and L respectively. Using the multiple variable regression function in Matlab, the values of i , j and A can be found by best fitting the data given in Table 2 (see Fig. 12), and **Eq. 4** can be expressed as

$$Re_n^{0.14} L^{2.3} Str = 18.5 \quad (5)$$

Judging from the relative magnitude of the exponents of the three dimensionless parameters in **Eq. 5**, one can see that over the range of Re_n examined in this paper, the net flow Reynolds number is less influential than the other two parameters. In addition, increasing the dimensional stroke length L is more effective than increasing the Strouhal number. The above

functional relationship can be used for selecting the synthetic jet operating conditions to ensure a good mixing between two laminar streams for a scaled version of this mixer.

3.5 The mechanisms of mixing

Based on the PLIF and PIV data we have gathered so far, synthetic jet pairs can enhance mixing by effectively increasing the interfacial area and the local dye concentration gradient via two key mechanisms: (a) Vortex interaction and entrainment; (b) Tearing and stretching of fluid elements, both of which are enabled and enhanced by the 180° out-of-phase actuation of periodic blowing and suction.

Vortex pairs are likely to be produced at a jet Reynolds number greater than 50 [19]. These vortex pairs entrained ambient fluid into their cores hence enhancing mixing. Vortex interaction, which leads to vortex distortion and even vortex break-up, is found to play an important role in promoting mixing at $Re_n=83$ and higher Reynolds numbers [12, 13]. It results in an excellent mixing obtained at such Reynolds numbers and a short mixing distance required for achieving a homogenous mixing at a high L . The vortex effect can be increased by increasing the jet Reynolds number with the use of a higher f or L .

It can be seen from Table 2 that due to the use of fluids with higher viscosities the values of Re_j are reduced significantly at $Re_n=2$ and 10 such that vortex rollup becomes impossible. The fact, that a very good mixing can be achieved in these cases, suggests that the effect of (b) can be very effective by itself and it is likely to remain to be effective at even lower net flow Reynolds numbers. In the present setup, partially mixed fluid is inhaled into a cavity within which further mixing takes places before it is subsequently ejected out of the cavity. With our multiple jet pair arrangement, a good mixing is guaranteed by forcing the fluid to go

through such a process three times. Furthermore, the benefit of tearing and stretching of fluid elements due to periodic blowing and suction is escalated by the out-of-phase operation of the synthetic jet pairs, which creates sequential segmentation of fluid with high and low dye concentration. Clearly, the effect of (b) can be enhanced by increasing the actuation frequency.

4. Summary

In the work reported in this paper, mixing between two fluid streams of the same flow rate in a planar mixing channel is enhanced using three lateral synthetic jet pairs respectively at a net flow Reynolds number of 2, 10 and 83. The changes in the flow Reynolds numbers are produced with the use of fluids with different dynamic viscosities. The synthetic jet pair is operated 180° out-of-phase and at a range of actuation frequencies and displacements. The extent of mixing in the mixing channel is examined using both PLIF and PIV.

It is found that at a sufficiently high frequency or dimensionless stroke length, a nearly homogenous mixing can be obtained. Our experimental evidence shows that synthetic jet pairs enhance mixing by effectively increasing the interfacial area and the local dye concentration gradient via two key mechanisms. While vortex interaction and entrainment plays an important role in promoting mixing at $Re_n=83$ and higher Reynolds numbers, tearing and stretching of fluid elements created by the ejection and ingestion cycles of the synthetic jets and sequential segmentation generated by the out-of-phase operation of the synthetic jet pairs are effective at the three Reynolds numbers examined here.

The degree of mixing is quantified using our PLIF data at a distance of $12.5h$ from the centre of the jet cavity. A functional relationship among Re_n , Str and L to ensure a nearly

homogenous mixing is also obtained by best fitting the experimental data. It can be used for selecting the synthetic jet operating conditions to ensure a good mixing for a scaled version of this fluid mixers. This correlation relationship indicates that the effectiveness of mixing is relatively insensitive to changes in Re_n implying that the fluid mixers of such a design can be effective over a wide range of net flow Reynolds numbers and for fluids of different viscosities.

Acknowledgements

The first author of this paper, Dr Qingfeng Xia, would like to acknowledge the financial support from both The University of Manchester and The Universities UK for his PhD studies.

Nomenclature

d	Width of synthetic jet orifice, m
f	Synthetic jet actuation frequency, Hz
h	Width of the mixing channel, m
L	Dimensionless stroke length
Re	Reynolds number
R_v	Velocity ratio
Str	Strouhal number
T	Period of synthetic jet actuation, s
U	Velocity, m/s
x, y, z	Coordinate, m

Greek symbols

ρ	Density, $kg.m^{-3}$
--------	----------------------

μ Dynamic viscosity, Pa.s

Subscript:

j Synthetic jet

n Net flow

References

1. Wong, S.H., M.C.L. Ward, and C.W. Wharton, *Micro T-mixer as a rapid mixing micromixer*. Sensors & Actuators: B. Chemical, 2004. **100**(3): p. 359-379.
2. Niu, X. and Y.K. Lee, *Efficient spatial-temporal chaotic mixing in microchannels*. Journal of Micromechanics and Microengineering, 2003. **13**(3): p. 454-462.
3. Paik, P., V.K. Pamula, and R.B. Fair, *Rapid droplet mixers for digital microfluidic systems*. Lab on a Chip, 2003. **3**(4): p. 253-259.
4. Hoffmann, M., M. Schluter, and N. Rabiger, *Experimental investigation of liquid-liquid mixing in T-shaped micro-mixers using μ -LIF and μ -PIV*. Chemical Engineering Science, 2006. **61**(9): p. 2968-2976.
5. Bothe, D., C. Stemich, and H.J. Warnecke, *Fluid mixing in a T-shaped micro-mixer*. Chemical engineering science, 2006. **61**(9): p. 2950-2958.
6. Zhou, J., H. Tang, and S. Zhong, *Vortex roll-Up criterion for synthetic jets*. AIAA Journal, 2009. **47**(5): p. 1252-1262.
7. Holman, R.U., Y.Mittal, R. Smith, B. L. Cattafesta, L., *Formation criterion for synthetic jets*. AIAA Journal, 2005. **43**(10): p. 2110-2116.
8. Glezer, A. and M. Amitay, *Synthetic jets*. Annual Review of Fluid Mechanics, 2002. **34**(1): p. 503-529.
9. Broučková, Z. and Z. Trávníček, *Visualization study of hybrid synthetic jets*. Journal of Visualization, 2014. **18**(4): p. 1-13.
10. Chaudhari, M., B. Puranik, and A. Agrawal, *Heat transfer characteristics of synthetic jet impingement cooling*. International Journal of Heat and Mass Transfer, 2010. **53**(5-6): p. 1057-1069.
11. Chaudhari, M., B. Puranik, and A. Agrawal, *Multiple orifice synthetic jet for improvement in impingement heat transfer*. International Journal of Heat and Mass Transfer, 2011. **54**(9), p.2056-2065.
12. Xia, Q. and S. Zhong, *A PLIF and PIV study of liquid mixing enhanced by a lateral synthetic jet pair*. International Journal of Heat and Fluid Flow, 2012. **37**: p. 64-73.
13. Xia, Q. and S. Zhong, *Enhancement of laminar flow mixing using a pair of staggered lateral synthetic jets*. Sensors and Actuators A: Physical, 2014. **207**(0): p. 75-83.
14. Xia, Q. and S. Zhong, *Liquids mixing enhanced by multiple synthetic jet pairs at low Reynolds numbers*. Chemical Engineering Science, 2013. **102**: p. 10-23.
15. Xia, Q., *Enhancement of liquids mixing using active pulsation in the laminar flow regime*. PhD dissertation, School of mechanical, Aerospace and Civil Engineering, Manchester University, 2012.
16. Glasgow, I. and N. Aubry, *Enhancement of microfluidic mixing using time pulsing*. Lab on a Chip, 2003. **3**(2): p. 114-120.
17. Quintas, M., et al., *Rheology of supersaturated sucrose solutions*. Journal of Food Engineering, 2006. **77**(4): p. 844-852.

18. Mageean, M.P., et al., *Physical properties of sugars and their solutions*. 1991: British Food Manufacturing Industries Research Association.
19. Xia, Q. and S. Zhong, *Quantification of liquid mixing enhanced by alternatively pulsed injection in a confined jet configuration*. *Journal of Visualization*, 2012. **15**(1): p. 57-66.

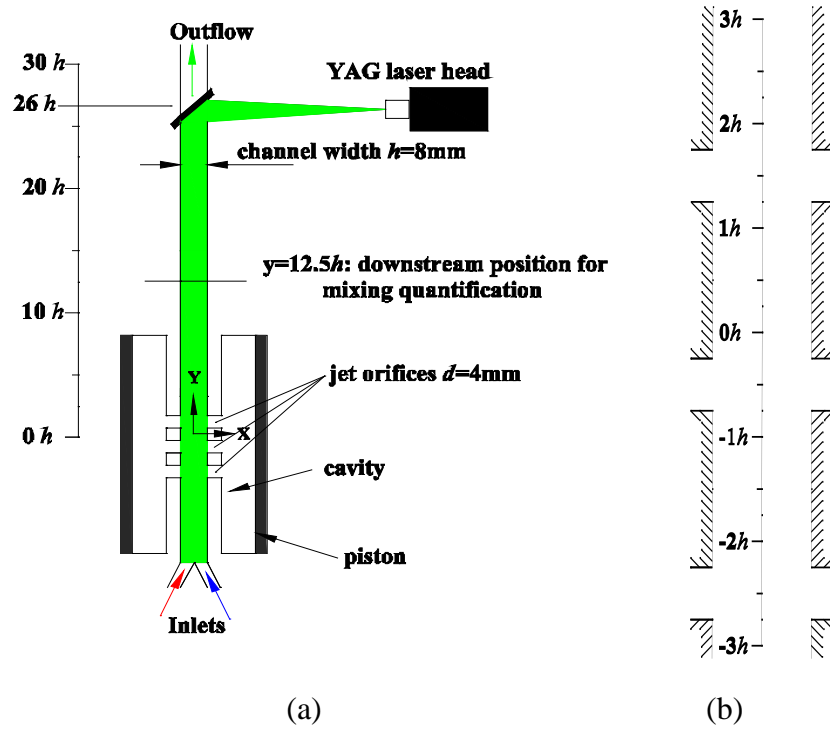


Fig. 1 (a) Schematic of the experimental set up for PIV and PLIF;
(b) Orifice arrangement for three synthetic jet pairs configuration.

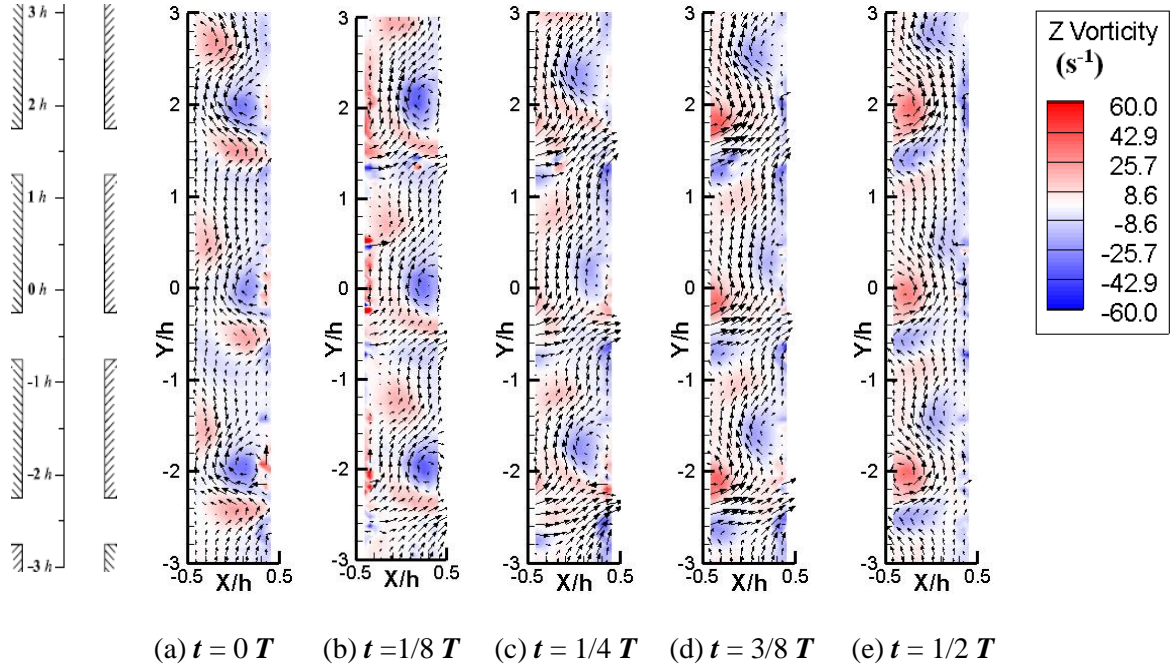


Fig. 2 Phase-averaged velocity vector field superimposed with vorticity contours during a synthetic jet actuation cycle at $L=4$, $Str=0.4$ ($f=1\text{Hz}$, $R_v=1.6$), $Re_n=83$

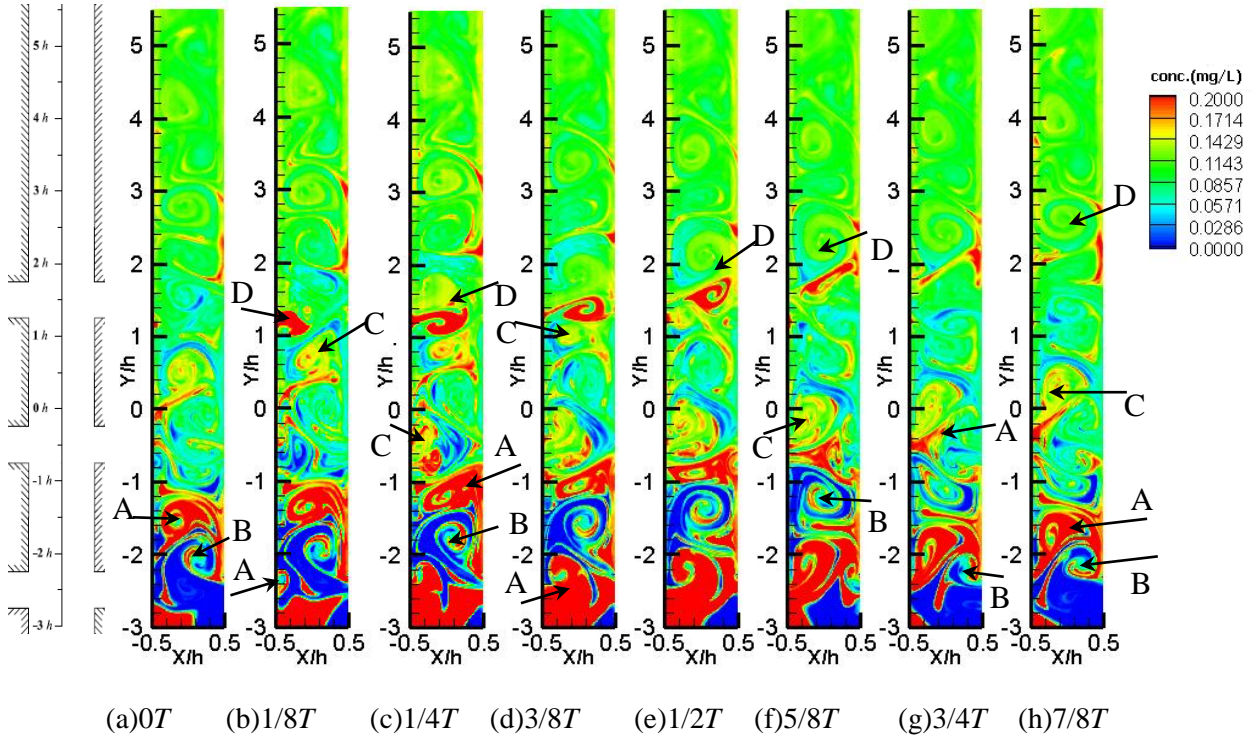


Fig. 3 A time sequence of instantaneous concentration contours during a synthetic jet actuation cycle at $L=4$, $Str=0.4$ ($f=1\text{Hz}$, $R_v=1.6$), $Re_n=83$

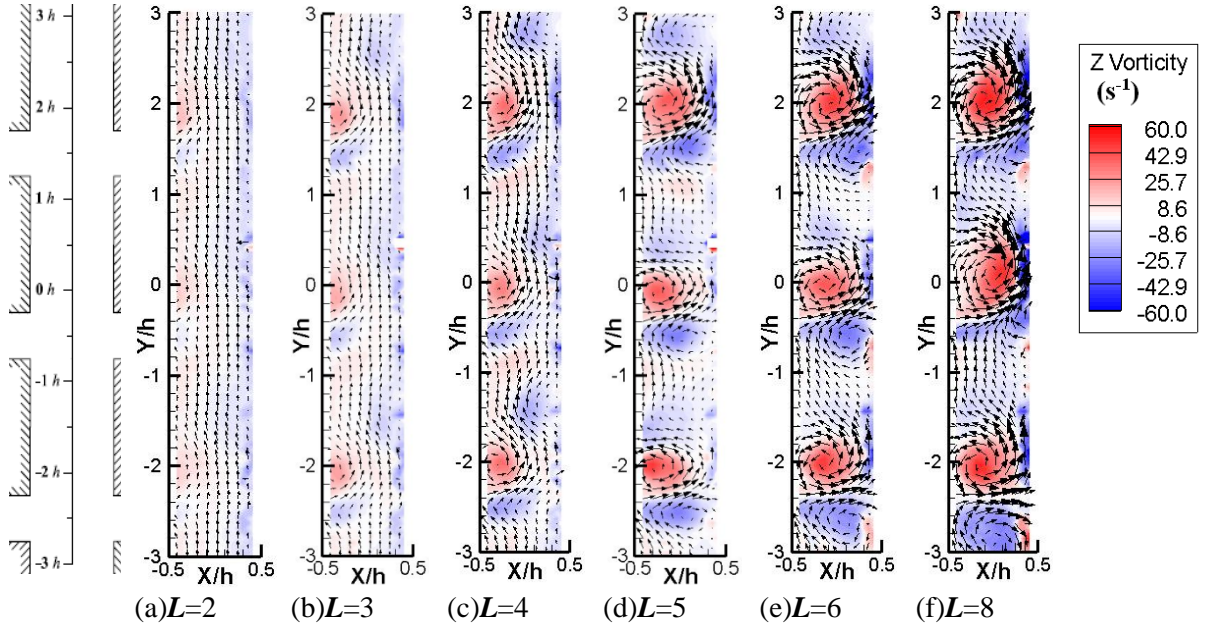


Fig. 4 Velocity vector fields superimposed with vorticity contours

at $t=1/2T$, $Str=0.4$ ($f=1\text{Hz}$) and $Re_n=83$

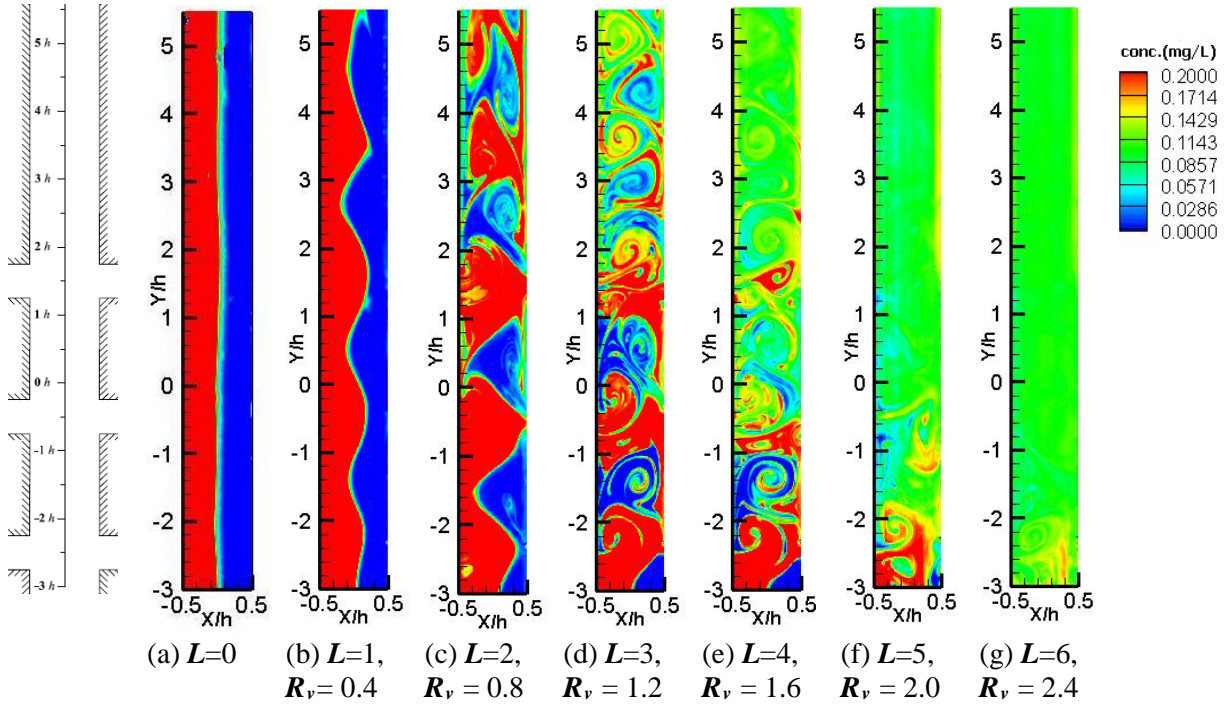


Fig. 5 Concentration contours at different L and at $t=1/2T$, $Str=0.4$ ($f=1\text{Hz}$), $Re_n=83$

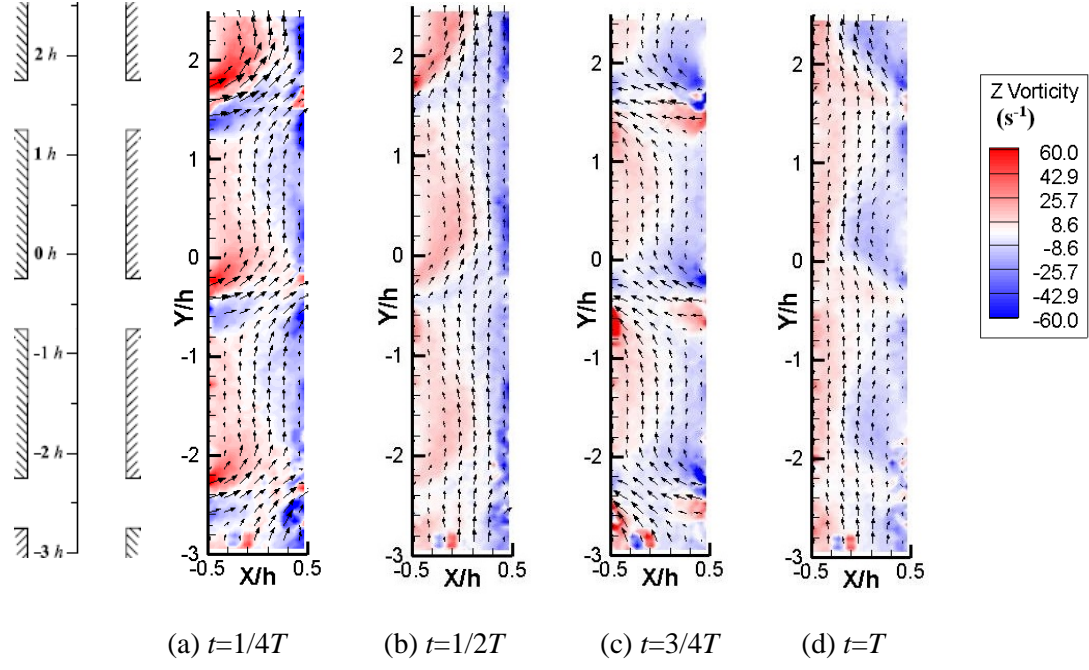


Fig. 6 Phase-averaged velocity vectors field superimposed with vorticity contours during a synthetic jet actuation cycle, $L=4$, $Str=0.4$ ($f=1\text{Hz}$, $R_v=1.6$), $Re_n=10$

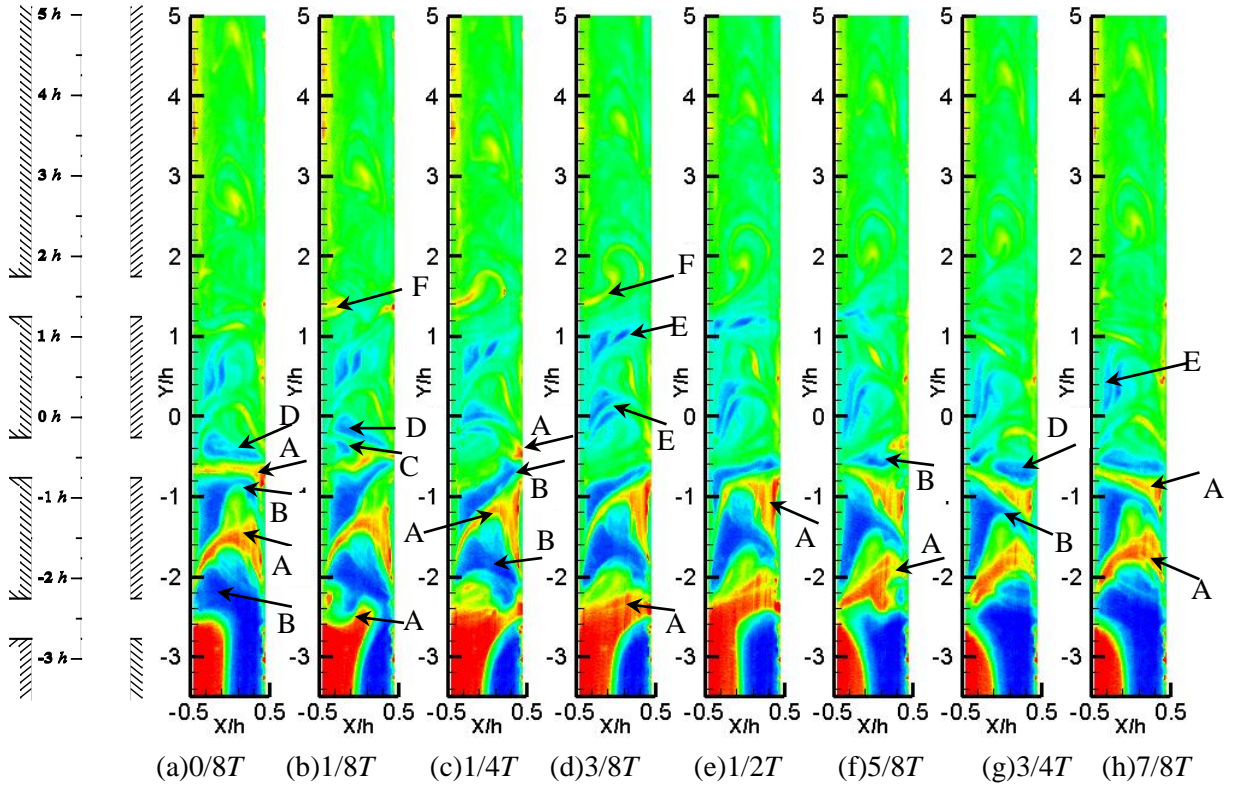


Fig. 7 Instantaneous dye concentration contours during a synthetic jet actuation cycle at $L=4$, $Str=0.4$ ($f=1\text{Hz}$), $Re_n=10$

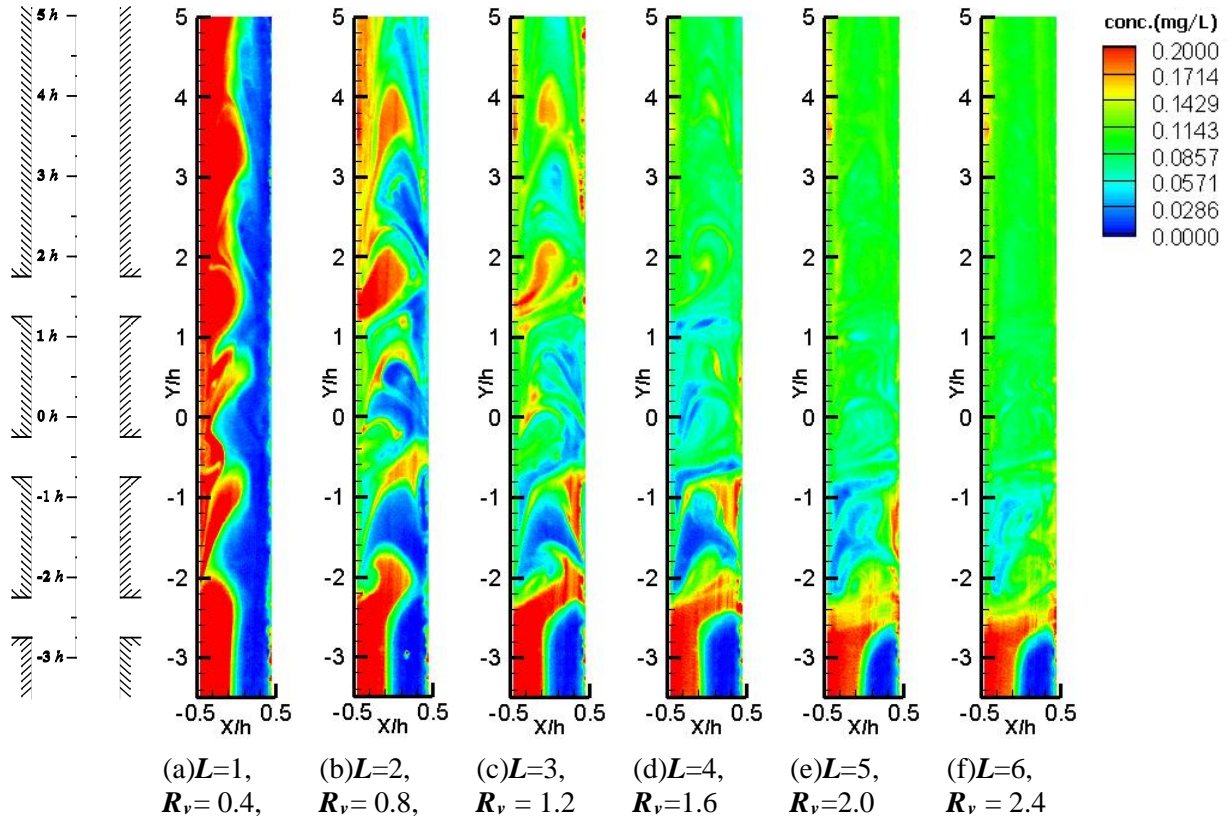
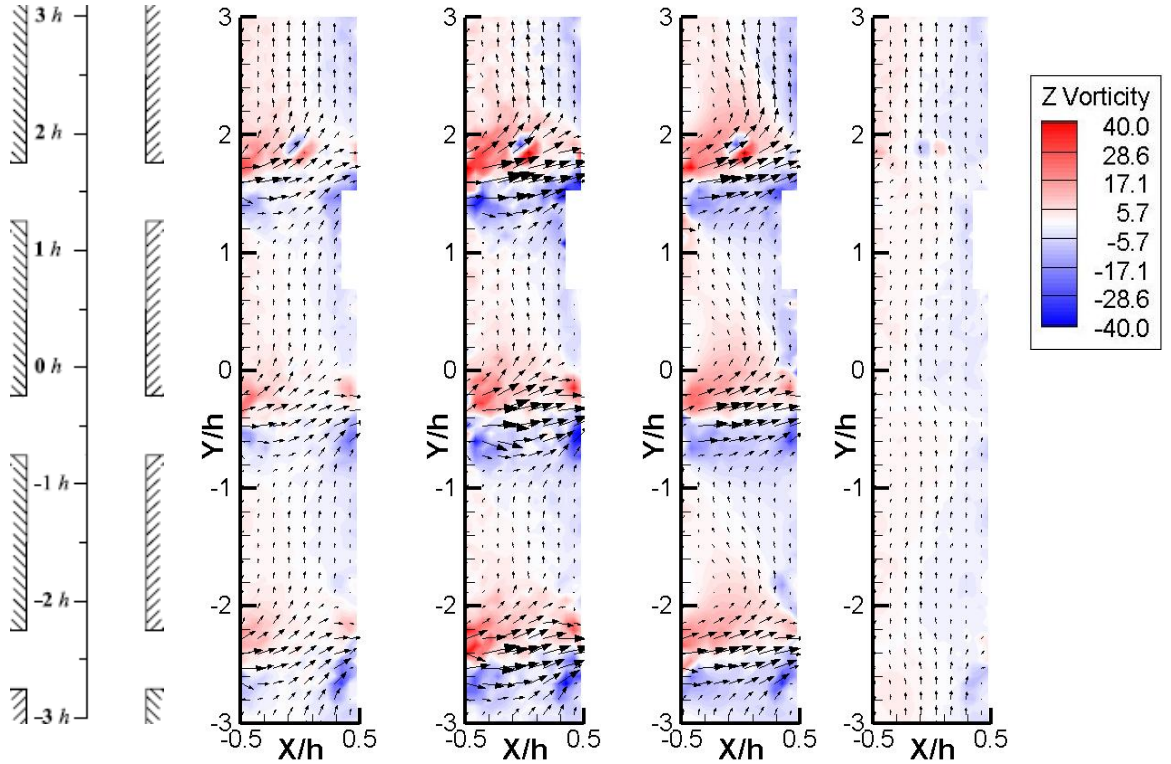


Fig. 8 Instantaneous dye contours at different L at $Str=0.4$ ($f=1\text{Hz}$), $t=T/2$, $Re_n=10$



(a) $t=1/8 T$ (b) $t=1/4 T$ (c) $t=3/8 T$ (d) $t=1/2 T$

Fig. 9 Phase-averaged velocity vector fields superimposed with vorticity contours during a synthetic jet actuation cycle at $L=6$, $Str=0.4$ ($f=1\text{Hz}$, $R_v=2.4$), $Re_n=2$

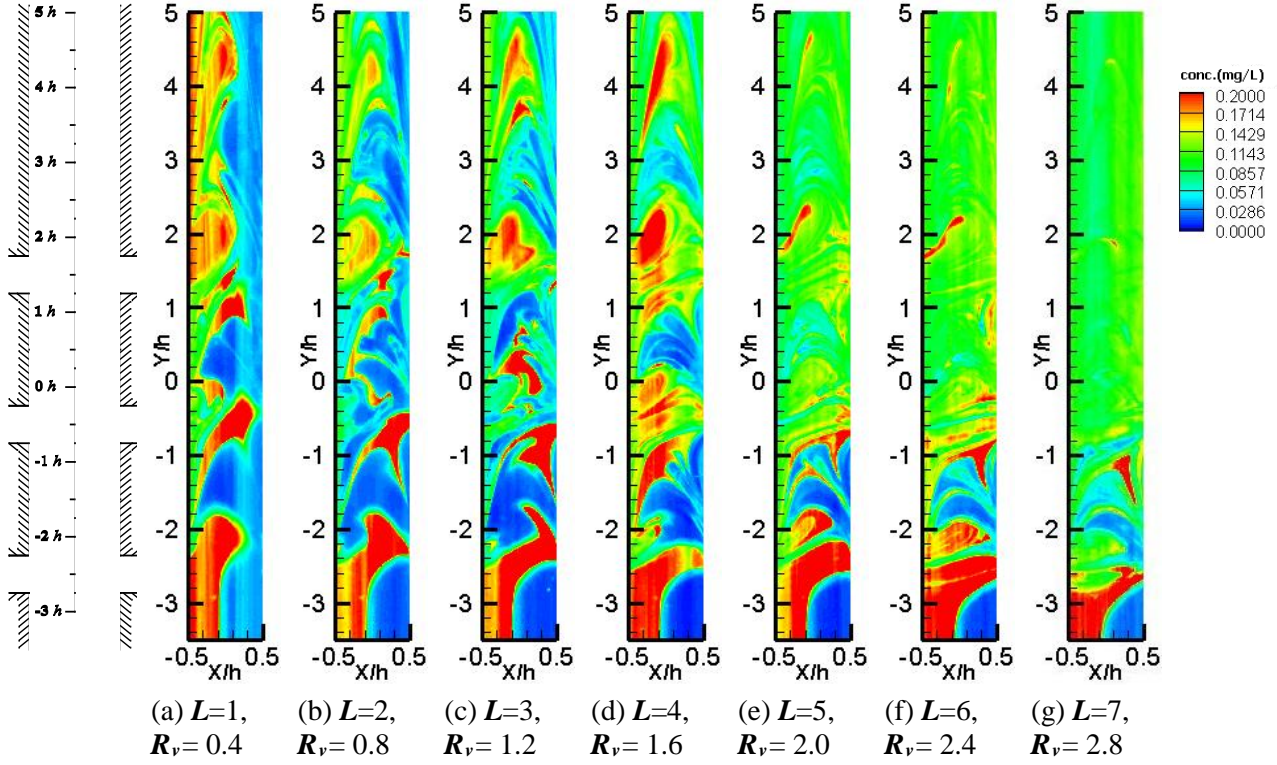


Fig. 10 Instantaneous dye concentration contours at different L at $Str=0.4$ ($f=1\text{Hz}$), $Re_n=2$

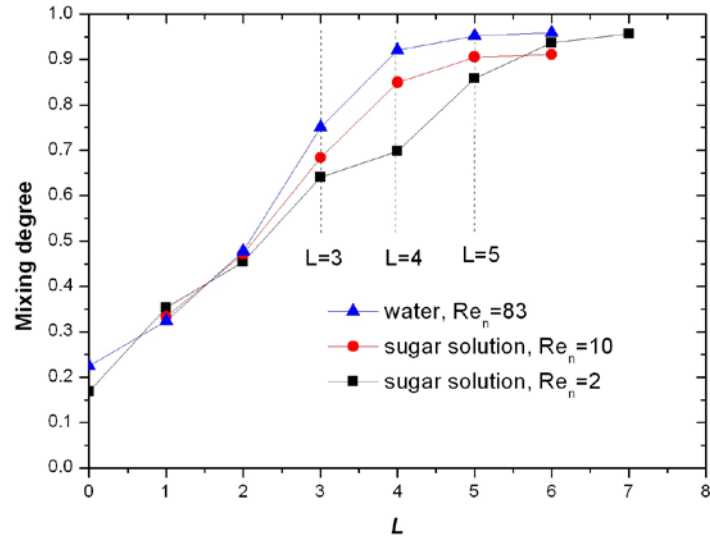


Fig. 11 Variations of degree of mixing with L at three different Re_n , $Str=0.4$ ($f=1$ Hz)

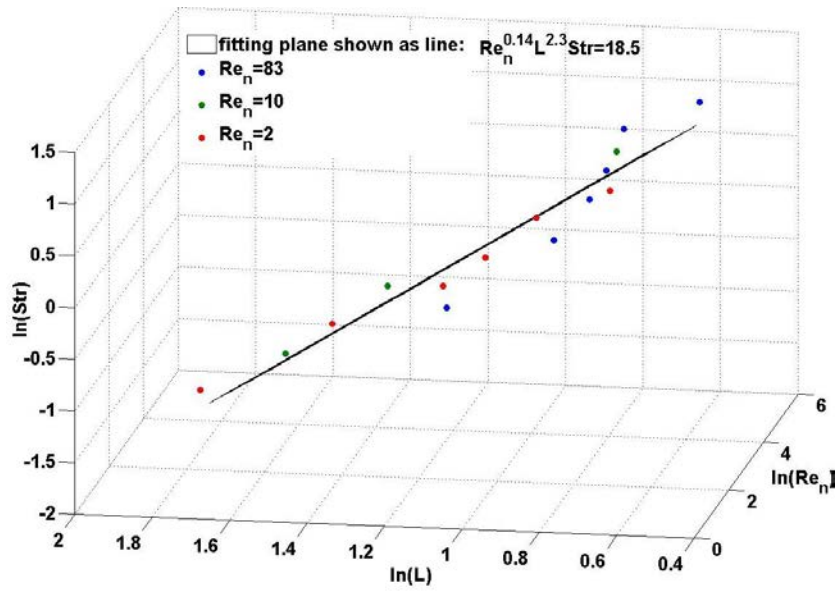


Fig. 12 Best fit of the functional relationship between Re_n , L and Str for good mixing